Testing a solar-blind pyrometer

2010 Metrologia 47 646

(http://iopscience.iop.org/0026-1394/47/6/003)

Metrologia **47** (2010) 646–651 doi:10.1088/0026-1394/47/6/003

Testing a solar-blind pyrometer

J Ballestrín, A Marzo, I Cañadas and J Rodríguez

CIEMAT–Plataforma Solar de Almería, Aptdo. 22, E-04200 Tabernas, Almería, Spain

Received 13 May 2010, in final form 6 September 2010
Published 4 October 2010
Online at stacks.iop.org/Met/47/646

Abstract
Surface temperatures are key parameters in many concentrated solar radiation applications. Pyrometric temperature measurement of solar irradiated material surfaces is the alternative to contact measurement techniques, which are inadequate for measuring the temperatures of such surfaces. However, reflected solar radiation is an important uncertainty variable in this non-contact methodology. A promising method for eliminating this solar perturbation is by using centred passband filters on the atmospheric solar absorption bands, creating solar-blind pyrometric systems. A commercial pyrometer has been tested in the wavelength band at around 1.4 µm in the solar furnace at Plataforma Solar de Almería, showing its advantages and limitations. An estimation of temperature measurement uncertainty for a real case is presented with theory and experiment in agreement: the higher the temperature, the lower the uncertainty. Another experiment has shown that the pyrometer measures temperature properly even through quartz windows in this spectral range.

(Some figures in this article are in colour only in the electronic version)

1. Introduction

Knowledge of surface temperatures is essential in many applications of concentrated solar radiation [1–6]. Pyrometric temperature measurement of solar irradiated material surfaces is a good alternative to contact metrology, which is not very advisable for measuring surface temperatures because:

- Heat is extracted if the surface is touched by the sensor.
- There is a strong dependence on the contact.
- Contact sensors have a very limited temperature range.

Pyroelectric detectors are the most common optical thermal detectors, as they are the most sensitive to thermal radiation and are fairly inexpensive. In these transducers, a change in temperature creates a change in polarization. Thus a pyroelectric device produces current only as it experiences a rise or fall in temperature. Pyrometric temperature determination is, however, distorted by reflected solar radiation from the irradiated sample. This problem is particularly important in solar furnaces where other alternative solutions have been proposed:

- By modulating the incident flux by an attenuator or shutter, the solar influence during the temperature measurement is controlled.
- Online determination of the incident flux and the sample spectral reflectivity [7].

Several authors have suggested the use of a pyrometer using bandpass filters centred on the atmospheric solar absorption bands [7–9] of carbon dioxide and atmospheric water. This procedure minimizes or avoids this source of uncertainty. On the other hand, determination of the real temperature requires knowledge of the surface emissivity as the temperature is determined on the basis of the current signal generated by the radiant surface compared with the signal generated by a blackbody calibrator. Although this subject is out of the scope of this study, the solar absorption band with the shortest wavelength has been chosen because the influence of the uncertainty of the emissivity on the surface temperature determination is less than with longer wavelengths [10].

This paper reports on a commercial pyrometer tested in the wavelength band around 1.4 µm in the solar furnace at the Plataforma Solar de Almería (PSA) in two different experiments in material treatment with concentrated solar radiation. This pyrometer has frequently been used for other concentrated solar radiation studies [1, 2, 4–6]. The good points and limitations of this device are presented in this paper.

2. PSA solar furnace

Solar furnaces reach the highest energy levels obtainable with a solar concentrating system, having attained concentrations of over 10 000X. A solar furnace essentially consists of a flat solar-tracking heliostat, a parabolic collector mirror,

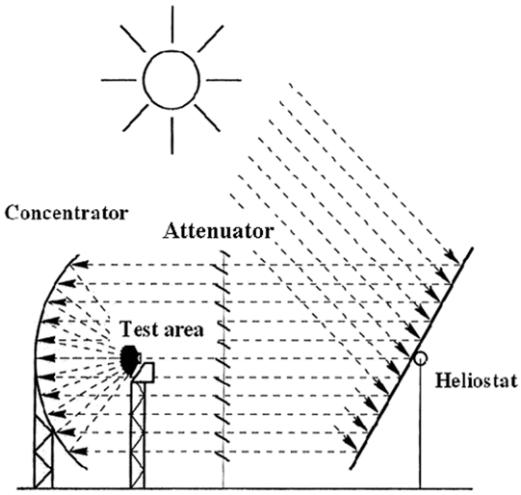

Figure 1. Solar furnace diagram.

Figure 2. The solar-blind pyrometer.

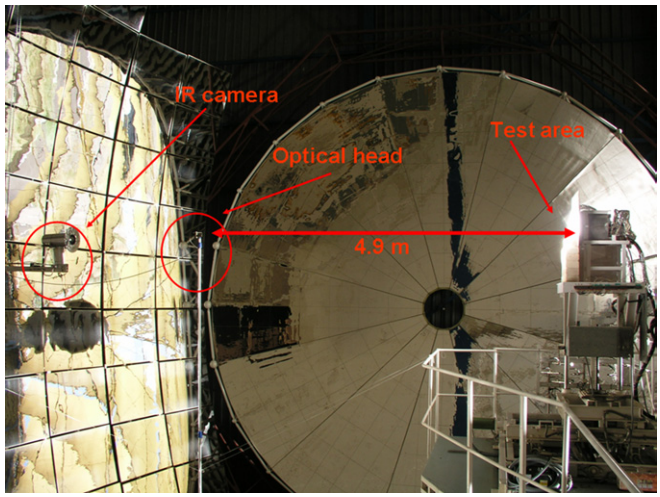

Figure 3. Pyrometer optical head and IR camera positions in the PSA solar furnace.

an attenuator or shutter and the test zone located at the concentrator focus (figure 1). The flat collector mirror, or heliostat, reflects the parallel horizontal solar beams onto the parabolic dish, which in turn reflects them onto the test area at its focus. The amount of incident light is regulated by the shutter located between the concentrator and the heliostat. There is a test table movable in three directions (East–West, North–South, up and down) under the focus that places the test samples at the focus with great precision.

The PSA solar furnace currently has one 140 m^2 heliostat. The reflective surface of the heliostat is made up of 32 non-concentrating flat facets with 90% reflectivity, which continually track the solar disc and reflect its parallel horizontal beams onto the concentrator. The concentrator dish is the main component of the solar furnace (figure 1). It concentrates the incident light from the heliostat, multiplying the radiant energy in the focal zone. Its optical properties especially affect the irradiance distribution at the focus. It is composed of 89 spherical facets with a total surface of 98.5 m^2, 92% reflectivity and a focal distance of 7.45 m. The parabolic surface is achieved with spherically curved facets, distributed along five radii with different curvatures depending on their distance from the focus. The attenuator consists of a set of horizontal louvers that rotate on their axes, regulating the amount of entering sunlight incident on the concentrator. The total energy at the focus is proportional to the radiation that passes through the attenuator. It is composed of 30 louvers arranged in two columns of 15. In closed position, the louvers form a 55° angle with the horizontal and 0° when open. The concentrator and distribution of the irradiance at the focus characterize a solar furnace. When 100% open with direct solar irradiance of 1000 W m^{-2}, peak irradiance at the focus [11] is 3034 kW m^{-2}, total power 69 kW and 90% power focal diameter of 26.2 cm.

3. Solar-blind pyrometer

The solar-blind pyrometer was developed by IMPAC Electronic GmbH in Germany in collaboration with the Paul Scherrer Institute [7] and has frequently been used for other concentrated solar radiation studies [1, 2, 4–6]. The solar-blind pyrometer shown in figure 2 is based on a standard industrial fibre optics IMPAC (Infratherm IGA 5LO) pyrometer. It is composed of an optical head, optical fibre (5 m), detector and the signal processing unit. The optical head contains no electronics, allowing for compact and robust construction (diameter: 25 mm, maximum operating temperature: 250 °C). The size of the sensitive area depends on the lens used and the distance. In our case, it is a circular spot 25.4 mm in diameter at a distance of about 4.9 m (figure 3), and as small as 0.45 mm in diameter at a distance of 87 mm. The signal processing unit is equipped with an InGaAs photodiode infrared detector and a narrow band filter (centre wavelength: 1398.0 nm, FWHM: 36.0 nm) changing the instrument's usual spectral response of 800 nm to 1800 nm to a small interval around 1400 nm. The range of measurable temperatures is from 500 °C to 2500 °C. Digital signal processing guarantees high accuracy (in absence of solar radiation: 0.3% for temperatures below 1500 °C, 0.5% above 1500 °C). Features include self-test functions, range zoom without recalibration, different outputs (serial interfaces, analogue outputs) and remote operation via personal computer. The IR camera also used for this work was a Flir Systems

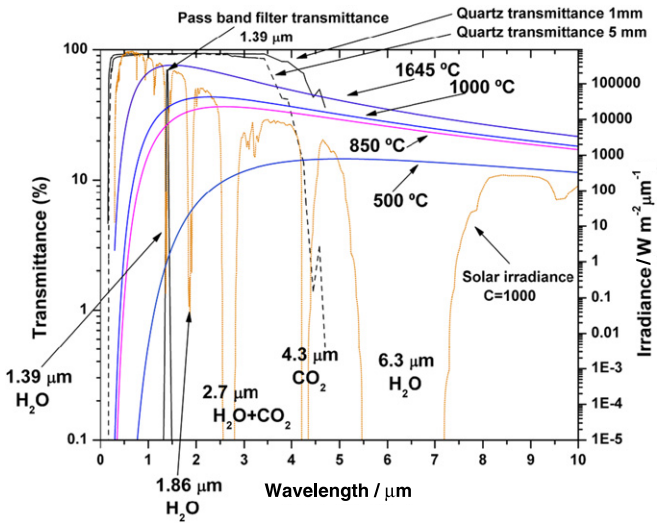

Figure 4. Atmospheric absorption solar bands in a concentrated solar spectrum based on a LOWTRAN simulation, blackbody radiance at several temperatures, passband filter transmittance at around 1.4 μm and quartz transmittances.

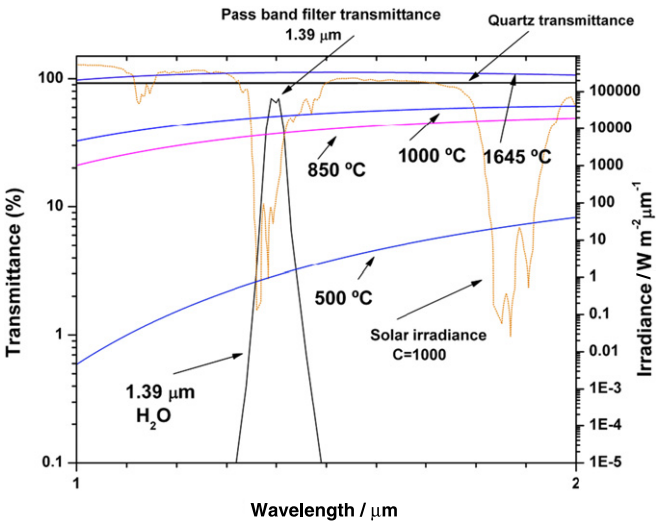

Figure 5. Atmospheric absorption solar band in a concentrated solar spectrum based on a LOWTRAN simulation, blackbody radiance at several temperatures, passband filter transmittance at around 1.4 μm and quartz transmittances.

(Model Thermacam SC 500) infrared digital video camera working in the 7.5 μm to 13 μm spectral range with bolometer technology which, in principle, would be affected by reflected solar radiation. The temperature range of the camera is −40 °C to 2000 °C with a minimal accuracy of ±2 °C, 14-bit digitalization, 12° lens and electronic zoom. Pyrometer and IR camera were calibrated using a MIKRON blackbody. The standards used for the calibration of the blackbody are traceable to the NIST.

3.1. Theoretical approach

Figure 4 shows the different atmospheric solar absorption bands in a concentrated solar spectrum based on a LOWTRAN code simulation [12], blackbody irradiance at several temperatures, passband filter transmittance of around 1.4 μm and quartz transmittance. Figure 5 shows the same information in the atmospheric solar absorption band at around 1.4 μm in more detail.

As shown in figure 5, the water absorption solar band at around 1.4 μm does not completely remove the solar radiation. This is the reason why the influence of water absorption along the path of radiation emitted from the surface up to the pyrometer (4.9 m) due to its own temperature is neglected. The blackbody irradiance in the passband filter wavelength range increases as the temperature of the body increases. As a result, the pyrometer measures better at higher surface temperatures. Figure 5 also shows the good quartz window transmittance (93%) of the solar radiation.

3.2. SiC experiment

A first experiment with the pyrometer described above was performed during the evaluation of a porous SiC front-face volumetric receiver (figure 6) at the PSA solar furnace. The volumetric receiver is made of a group of porous SiC cups. These porous cups improve the penetrability of the solar

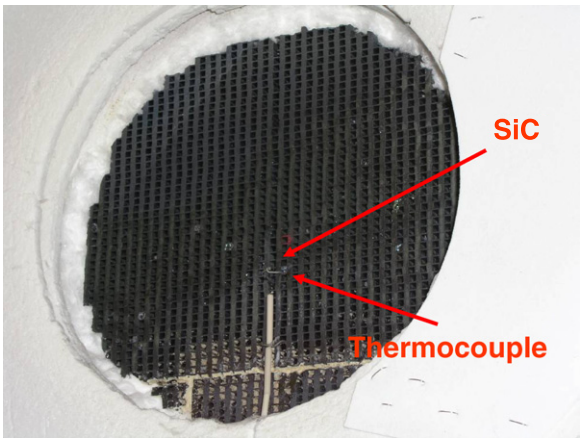

Figure 6. Volumetric receiver front face showing SiC porous cups and thermocouple.

radiation and increase the contact surface of the receiver with the solar radiation, giving a more efficient solar device. The air cooling process absorbs external air from a blower through the porous cups. The front-face receiver temperature under concentrated solar radiation was measured simultaneously with the pyrometer and a type-K thermocouple with calibration traceability to UKAS (−30 °C to 1370 °C). The thermocouple accuracy is ±2.5 °C and it is placed at 5 mm from the receiver back surface in contact with SiC (figure 7). Both measurements were taken at the same point. The SiC emissivity ($\varepsilon = 0.95$) is estimated from the spectral reflectivity of a sample ($\varepsilon = \alpha = 1 - \rho$) measured with a Perkin–Elmer Lambda 9 spectrophotometer in the 300 nm to 2500 nm spectral range. The measurements are compared in figure 8 before the thermocouple broke due to excessive temperature. As theoretically expected, agreement between the measurements is good at high temperatures. Figure 8 shows the pyrometer and type-K thermocouple measurements, where ΔT is the difference between the two measurements. The theoretical

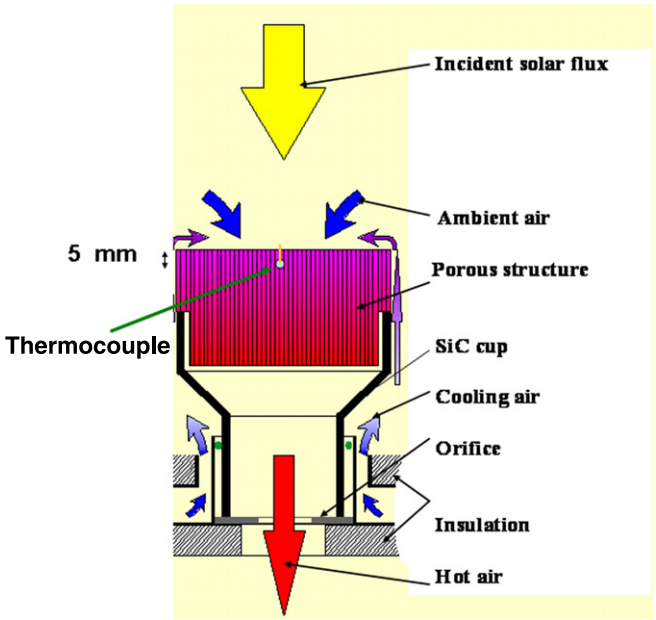

Figure 7. Thermocouple detail on the SiC cup.

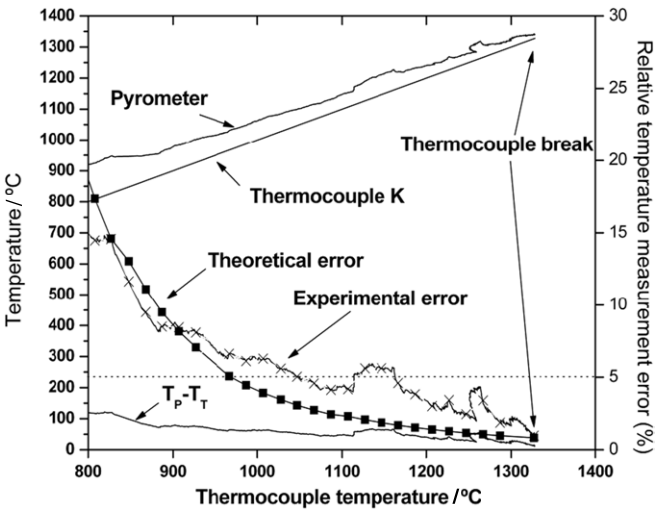

Figure 8. Comparison of pyrometer (T_P) and thermocouple (T_T) temperature measurements during the SiC experiment at PSA solar furnace. Experimental error against theoretical error.

relative error estimate considers the blackbody irradiance at different temperatures and the reflected solar radiation during the test. The blackbody irradiance through the passband filter of the pyrometer, $E_{b\lambda,1400}$, is obtained by the Planck law:

$$E_{b\lambda,1400} = \int_0^\infty \tau_{\lambda,1400} E_{b\lambda}\, d\lambda = \int_{800}^{1800} \tau_{\lambda,1400} \frac{C_1}{(e^{C_2/n\lambda T} - 1)\lambda^5 n^2}\, d\lambda, \quad (1)$$

$$C_1 = 3.74 \times 10^{20}\ \mathrm{W\,nm^4\,m^{-2}},$$

$$C_2 = 1.44 \times 10^7\ \mathrm{nm\,K},$$

where $\tau_{\lambda,1400}$ is the spectral transmittance of the passband filter centred on 1400 nm. The solar radiation reflected through the passband filter of the pyrometer, E_{ref}, is obtained as

Table 1. Relative error in the pyrometer temperature measurement for different blackbody temperatures (distance = 4.9 m). Relative humidity = 38%; ambient temperature = 30 °C.

Blackbody temperature T_{BB}/°C	600	750	900
Pyrometer temperature T_P/°C	588	734	883
100× Relative error in the temperature, $(T_P - T_{BB})/T_{BB}$	−2.0	−2.1	−1.9

$$E_{ref} = H f_a \int_{800}^{1800} E_{s\lambda}\, \tau_{\lambda,total}\, d\lambda, \quad (2)$$

where f_a is the shutter attenuation factor, which was 0.9 during the experiments with the pyrometer, $E_{s\lambda}$ is the solar spectral irradiance, H is the concentration factor obtained between the heliostat effective surface, A_{ef}, and the 90% of the focus surface, A_{focus}, on the test area (figure 1):

$$H \equiv 0.9 \frac{A_{ef}}{A_{foco}}. \quad (3)$$

The overall transmittance of the solar irradiance from the heliostat to the pyrometer, $\tau_{\lambda,total}$, is obtained as

$$\tau_{\lambda,total} \equiv \rho_{\lambda,heliostat}\, \rho_{\lambda,concentrator}\, \tau_{\lambda,1400}\, \rho_{\lambda,SiC}, \quad (4)$$

where $\rho_{\lambda,i}$ is the spectral reflectivity of the heliostat, concentrator and SiC, respectively.

The theoretical relative error estimate is finally obtained as

Irradiance relative error

$$= \frac{(E_{b\lambda,1400} + E_{ref}) - E_{b\lambda,1400}}{E_{b\lambda,1400}} = \frac{E_{ref}}{E_{b\lambda,1400}}. \quad (5)$$

The experimental relative error estimate considers the pyrometer and thermocouple measurements. The solar-blind selection of the spectral range inevitably leads to an influence of the atmosphere [7, 9] during temperature measurement with the pyrometer. In order to analyse the attenuation of thermal radiation, a blackbody calibration source (Mikron M305) has been placed in the focal plane on the solar furnace mobile test table. The optical head of the pyrometer is placed 4.9 m from the blackbody aperture (figure 3) and measures the temperature through the orifice. The distance from the blackbody during the original calibration of the pyrometer was 1 m. The relative humidity (38%) and the ambient temperature (30 °C) measurements were performed with a Testo 608H2 sensor. The spherical cavity in the blackbody yields an emissivity of 0.995 over the temperature range 100 °C to 1000 °C with an aperture of 25 mm and reading accuracy of ±0.25%. Table 1 shows the relative error in the pyrometer temperature (equation (6)), measured with the pyrometer, T_P, when the temperature of the blackbody, T_{BB}, is 600 °C, 750 °C and 900 °C, the relative humidity (38%) and the ambient temperature (30 °C). In all cases the relative error in the pyrometer temperature is around 2%. Local changes in

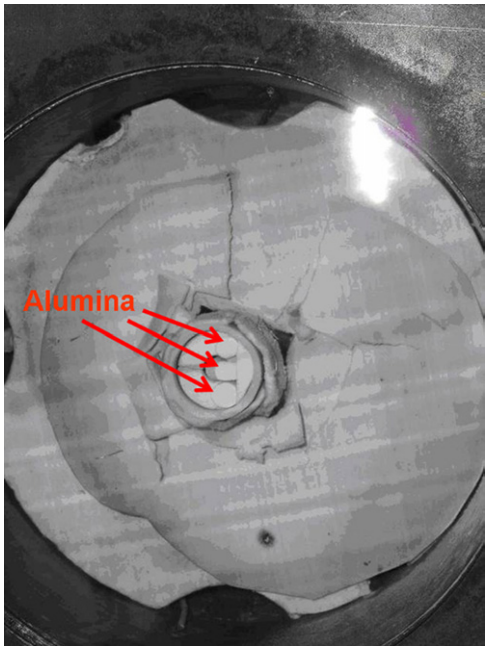

Figure 9. Cylinders of alumina protected by a porous zirconia blanket in an argon atmosphere under a quartz window.

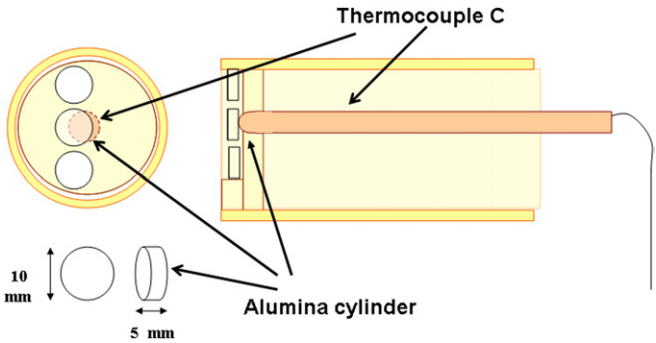

Figure 10. Cylinders of alumina protected by a porous zirconia blanket. Thermocouple detail.

relative humidity (±20%) and ambient temperature (±30%) have shown no significant changes in the relative error of the temperature measurement performed with the pyrometer at a distance of 4.9 m. The error introduced by the pyrometer has been corrected accordingly (figures 8, 11).

$$\text{Pyrometer temperature relative error} = \frac{T_{\mathrm{P}} - T_{\mathrm{BB}}}{T_{\mathrm{BB}}}. \qquad (6)$$

The theoretical and experimental errors are approximately 5% at 950 °C and exponentially decrease at higher temperatures. Below this temperature, the solar influence distorts the pyrometer's detection of thermal radiation. At higher temperatures, the solar influence is negligible compared with thermal radiation in the filter wavelength band around 1.4 µm (figures 4, 5).

3.3. Alumina experiment

A solar furnace is an ideal facility for sintering alumina at high temperatures even in a controlled atmosphere. Figure 9 shows

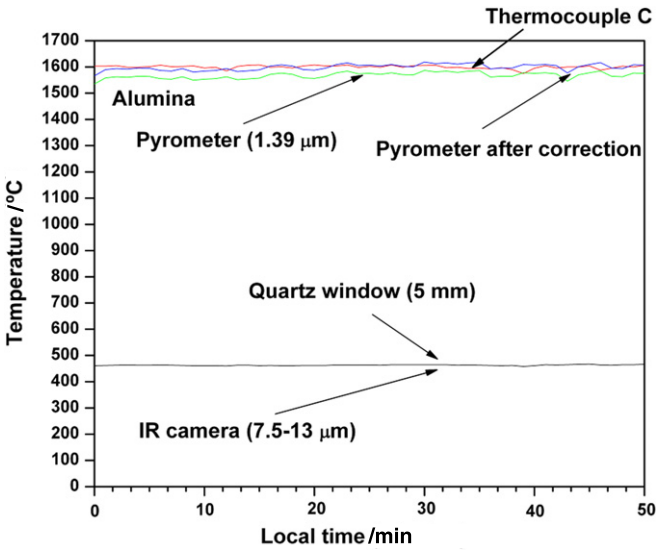

Figure 11. Pyrometer, thermocouple C and IR camera temperature measurements during the alumina test at PSA solar furnace.

three alumina cylinders protected by a porous zirconia blanket in an argon atmosphere to prevent the oxidation reaction during the test behind a quartz window. Zirconia is ideally suited for thermal insulation applications under conditions of ultra-high temperatures and in a variety of severe environments. The quartz window (5 mm thick) transmittance is 93% in the spectral working range of the pyrometer (figures 4, 5). The alumina surface temperature was measured simultaneously at the same point with the pyrometer and a type-C thermocouple. The thermocouple accuracy is ±4.5 °C and it is placed at 5 mm from the alumina back surface (figure 10). The temperature of the quartz window is measured with the infrared camera. The emissivities of alumina ($\varepsilon = 0.40$) and quartz ($\varepsilon = 0.80$) were acquired from the literature [13, 14]. High quartz transmittance in the working spectral range of the pyrometer makes temperature measurement of the alumina with this system possible. In contrast, the low transmittance of the quartz window in the working spectral range of the IR camera (figures 4, 5) allows the temperature of the window itself to be measured but makes measurement of the alumina temperature impossible. Figure 11 shows these measurements during a test of almost 1 h, where the temperature reached in the alumina is around 1600 °C. At this temperature, the solar influence in the pyrometer is negligible and the temperature measurement with this system is in agreement with the thermocouple measurement. The temperature measurement performed with the pyrometer must be increased using Planck's law correction due to the quartz attenuation (93%) of the detected thermal radiation.

4. Conclusions and outlook

Pyrometric temperature measurement of solar irradiated material surfaces is a good alternative to contact metrology. Pyrometric temperature determination is, however, distorted by solar radiation reflected from the irradiated sample. The use of pyrometry using bandpass filters centred on the atmospheric

solar absorption band of carbon dioxide and atmospheric water could minimize or avoid this source of uncertainty. This paper reports on a commercial pyrometer that has been tested in the wavelength band around 1.4 µm in the PSA solar furnace during two different concentrated solar materials treatment experiments. Theoretical and experimental error estimates have shown that under concentrated solar radiation conditions the pyrometer measurements have a relative error of approximately 5% at temperatures over 950 °C even through quartz windows and exponentially decrease at higher temperatures. This work will be followed by definition of an infrared camera that can work in different atmospheric solar absorption bands, in particular the bands centred at 2.7 µm and 4.3 µm where there is no solar contribution.

Acknowledgments

Thanks are due to Dr Andreas Neumann for the LOWTRAN simulation-based solar spectrum data.

References

[1] Schaffner B *et al* 2003 Recycling of hazardous solid waste material using high-temperature solar process heat: II. Reactor design and experimentation *Environ. Sci. Technol.* **37** 165–70

[2] Kraupl S and Steinfeld A 2003 Operational performance of a 5-kW solar chemical reactor for the co-production of zinc and syngas *Trans. ASME, J. Sol. Energy Eng.* **125** 124–6

[3] Hernandez D *et al* 2003 Evaluation of the application of a solar furnace to study the suitability of metal oxides to be used as secondary reference points in the range 2000–3000 °C *Measurement* **34** 101–9

[4] Meier A *et al* 2004 Design and experimental investigation of a horizontal rotary reactor for the solar thermal production of lime *Energy* **29** 811–21

[5] Osinga T *et al* 2004 Experimental investigation of the solar carbothermic reduction of ZnO using a two-cavity solar reactor *Trans. ASME, J. Sol. Energy Eng.* **126** 633–7

[6] Hirsch D and Steinfeld A 2004 Solar hydrogen production by thermal decomposition of natural gas using a vortex-flow reactor *Int. J. Hydrog. Energy* **29** 47–55

[7] Tschudi H R and Morian G 2001 Pyrometric temperature measurements in solar furnaces *Trans. ASME, J. Sol. Energy Eng.* **123** 164–70

[8] Hernandez D *et al* 2004 Analysis and experimental results of solar-blind temperature measurements in solar furnaces *Trans. ASME, J. Sol. Energy Eng.* **126** 645–53

[9] Pfänder M *et al* 2006 Pyrometric temperature measurements on solar thermal high temperature receivers *Trans. ASME, J. Sol. Energy Eng.* **128** 285–92

[10] Rohner N and Neumann A 2003 Measurement of high temperatures in the DLR solar furnace by UV-B detection *Trans. ASME, J. Sol. Energy Eng.* **125** 152–8

[11] Rodríguez J *et al* 2006 The PSA solar furnace: a facility ready to characterize high-concentration solar devices from solar thermal applications to PV cells *13th Int. Symp. on Concentrated Solar Power & Chemical Energy Technologies (Seville, Spain, 20–23 June 2006)*

[12] Kneizys F X, Shettle E P and Abreu L W 1988 User guide to LOWTRAN 7, Air Force Geophysics Laboratory, AFGL-TR-88-0177 Environmental Research Papers, No 1010

[13] McConnell B G 1999 A coupled heat transfer and electromagnetic model for simulating microwave heating of thin dielectric materials in a resonant cavity *PhD Thesis* Virginia Polytechnic Institute

[14] Ting A 1994 The influence of wavelength-dependent radiation simulation of lamp-heated rapid thermal processing systems, Sandia National Laboratories, CA 94551